

## Electronic Supplementary Information

### Ultrahigh permeable and selective nanofiltration membrane mediated by in-situ formed interlayer†

Yufan Hao,<sup>a</sup> Quan Li,<sup>a</sup> Benqiao He,<sup>\*a</sup> Bo Liao,<sup>b</sup> Xianhui Li,<sup>c</sup> Mengyang Hu,<sup>a</sup>  
Yanhong Ji,<sup>a</sup> Zhenyu Cui,<sup>a</sup> Mohammad Younas,<sup>a,d</sup> and Jianxin Li,<sup>\*a</sup>

<sup>a</sup>State Key Laboratory of Separation Membranes and Membrane Processes,  
School of Materials Science and Engineering, Tiangong University,  
Tianjin 300387, China

<sup>b</sup>School of Materials Science and Engineering, Hunan University of Science  
and Technology, Xiangtan, 411201, China

<sup>c</sup>Department of Chemical and Biochemical Engineering, Søtofts Plads,  
Building 229, Technical University of Denmark, DK-2800 Lyngby, Denmark

<sup>d</sup>Department of Chemical Engineering, University of Engineering and  
Technology, Peshawar, 25120, Pakistan

Email: hebenqiao@tjpu.edu.cn; jxli@tjpu.edu.cn

## Supplementary contents

(1) Live Video of Separation Performance .....	3
(2) Chemical Compositions of Chitosan Particles and Membranes.....	3
(3) Total Organic Carbon Concentration of Aqueous Amine Solution.....	4
(4) FESEM and TEM Micrographs of CSPs .....	5
(5) Surface and Cross-sectional Morphologies of PES/SPSf Ultrafiltration Membrane .....	5
(6) Surface Roughness Parameters of Membranes .....	6
(7) Surface Properties of Membranes .....	7
(8) Chemical Structure and Mechanism Diagram of Interfacial Polymerization.....	9
(9) Calculating Crosslinking Degree of PA layer .....	9
(10) Hydrophilicity and Zeta Potential of the Membranes .....	10
(11) Cross-sectional Morphologies of Membranes .....	11
(12) Relationship between Viscosity of Aqueous Amine Solution and the Thickness of PA Active Layer Obtained .....	12
(13) Experiment Setup of Membrane Separation and Pore Size of Membranes .....	13
(14) Separation Performance to Different Inorganic Salts.....	14
(15) Effect of pH of Feed Solution on Salt Separation Performance .....	16
(16) Surface Roughness, Active Layer Thickness and Separation Performance of PIP/TMC, PIP-CSP <sub>0</sub> /TMC and PIP-CSP <sub>6</sub> /TMC Membranes .....	17
(17) Mechanical Strength of Membranes .....	18
(18) Comparison of Filtration Performance with NF membranes Reported in Literature and Commercial NF Membrane. ....	19
(19) Stability Evaluation .....	20
(20) Relationship between Aqueous Amine Solution with Different pH and Separation Performance of the Corresponding Membranes .....	22
(21) Antifouling Property Evaluation .....	22
(22) Antibacterial Property Evaluation .....	25
References.....	27

## (1) Live Video of Separation Performance

The flux and rejection of 1 g/L  $\text{Na}_2\text{SO}_4$  solution were tested for PIP-CSP<sub>6</sub>/TMC and PIP/TMC membrane under 5 bar, respectively. The test process and results were shown as the video:



Live Video.wmv

## (2) Chemical Compositions of Chitosan Particles and Membranes

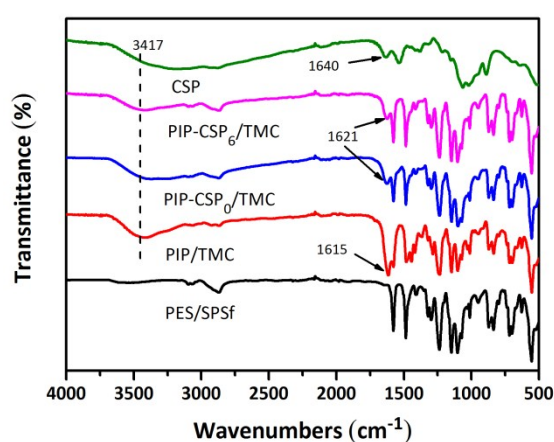


**Fig. S1.** FTIR spectra of CSPs, PES/SPSf, PIP/TMC and PIP-CSP/TMC membranes.

Chemical compositions of chitosan particles and membranes were characterized with Fourier transform infrared spectroscopy (FT-IR, Nicolet-IS50, USA). As shown in Fig. S1, new peaks were found at 1615  $\text{cm}^{-1}$  and 1621  $\text{cm}^{-1}$  ascribed to C=O (amide I) stretching vibrations of the PIP/TMC and PIP-CSP/TMC membranes, respectively, comparing with PES/SPSf membrane. It indicates that the interfacial polymerization occurred on the surface of PES/SPSf membrane. The vibration band of -OH or -NH (about 3417  $\text{cm}^{-1}$ ) confirmed the presence of hydrophilic functional groups on the free CS molecules, CSPs, PIP/TMC and PIP-CSP/TMC membranes.

### (3) Total Organic Carbon Concentration of Aqueous Amine Solution

**Table S1**

The ratio of free CS and CSPs in the aqueous amine solution calculated through organic carbon concentration.

Solution	Organic carbon conc. (g/L)			Ratio of free CS/CSPs
	Supernatant after centrifugation <sup>a)</sup>	Free CS <sup>b)</sup>	CSPs <sup>c)</sup>	
HAc+CS+PIP-0h	18.28	1.61	0.25	6.44
HAc+CS+PIP-2h	17.80	1.13	0.73	1.55
HAc+CS+PIP-4h	17.58	0.91	0.95	0.96
HAc+CS+PIP-6h	17.50	0.83	1.03	0.81
HAc+CS+PIP-8h	17.51	0.84	1.02	0.82

<sup>a)</sup> Centrifugation conditions are the speed of 14500 r/min for 1 h at 25°C;

<sup>b)</sup> The organic carbon (C) of free CS in the supernatant solution = the total organic carbon in supernatant solution -  $C_{\text{HAc}}$  (7.14 g/L) -  $C_{\text{PIP}}$  (9.53 g/L); the values of  $C_{\text{HAc}}$  and  $C_{\text{PIP}}$  were obtained by a TOC Analyzer, respectively.

<sup>c)</sup>  $C_{\text{CSPs}} = C_{\text{CS}}$  (1.86 g/L) -  $C_{\text{free CS}}$ ; the values of  $C_{\text{CS}}$  was obtained by a TOC Analyzer.

#### (4) FESEM and TEM Micrographs of CSPs

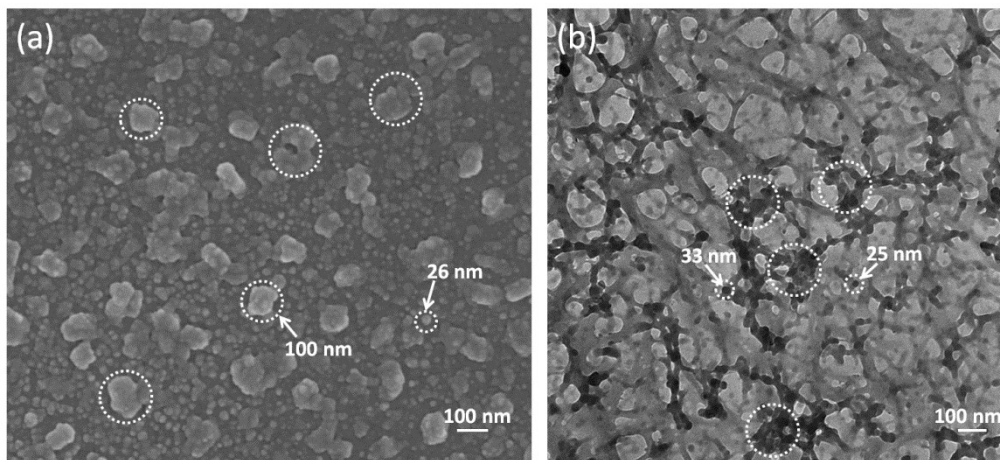


**Fig. S2.** (a) FESEM and (b) TEM micrographs of CSP in amine aqueous solution (prepared by 0.5 % CS and aged for 6 h) of diluted 10-fold on copper mesh dried at  $-45^{\circ}\text{C}$  for 24 h.

#### (5) Surface and Cross-sectional Morphologies of PES/SPSf Ultrafiltration Membrane

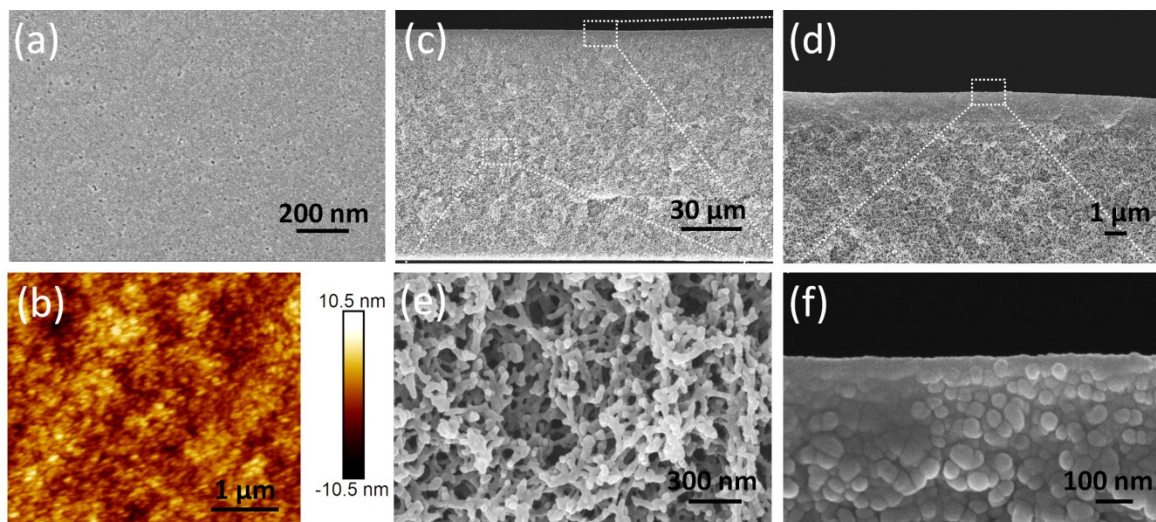


**Fig. S3.** Surface and cross-sectional morphologies of PES/SPSf membrane. (a) surface morphology by FESEM, and (b) surface morphology by AFM. (c-f) cross-sectional morphologies by FESEM.

## (6) Surface Roughness Parameters of Membranes

**Table S2**

Surface roughness and surface area of PES/SPSf, PIP/TMC and PIP-CSP/TMC membranes with different CS concentration and aging time.

Membrane	Surface parameters*			
	Ra (nm)	Rq (nm)	Rz (nm)	Surface area ( $\mu\text{m}^2$ )
PES/SPSf	1.6	2.0	15.2	25.0
PIP/TMC	6.2	8.3	79.9	25.2
0.25 wt% CS-0h	3.1	4.0	47.5	25.1
0.50 wt% CS-0h	4.4	5.6	42.3	25.1
0.75 wt% CS-0h	4.0	5.0	41.4	25.2
1.00 wt% CS-0h	5.3	7.0	81.6	25.2
0.50 wt% CS-2h	14.9	19.9	228	25.4
0.50 wt% CS-4h	17.0	24.0	196	25.3
0.50 wt% CS-6h	27.4	36.3	270	26.5
0.50 wt% CS-8h	42.7	55.7	338	26.3

\*The roughness and surface areas from a specific given size membrane ( $5*5 \mu\text{m}^2$ ) were measured by AFM (Bruker Dimension Icon, USA).

## (7) Surface Properties of Membranes

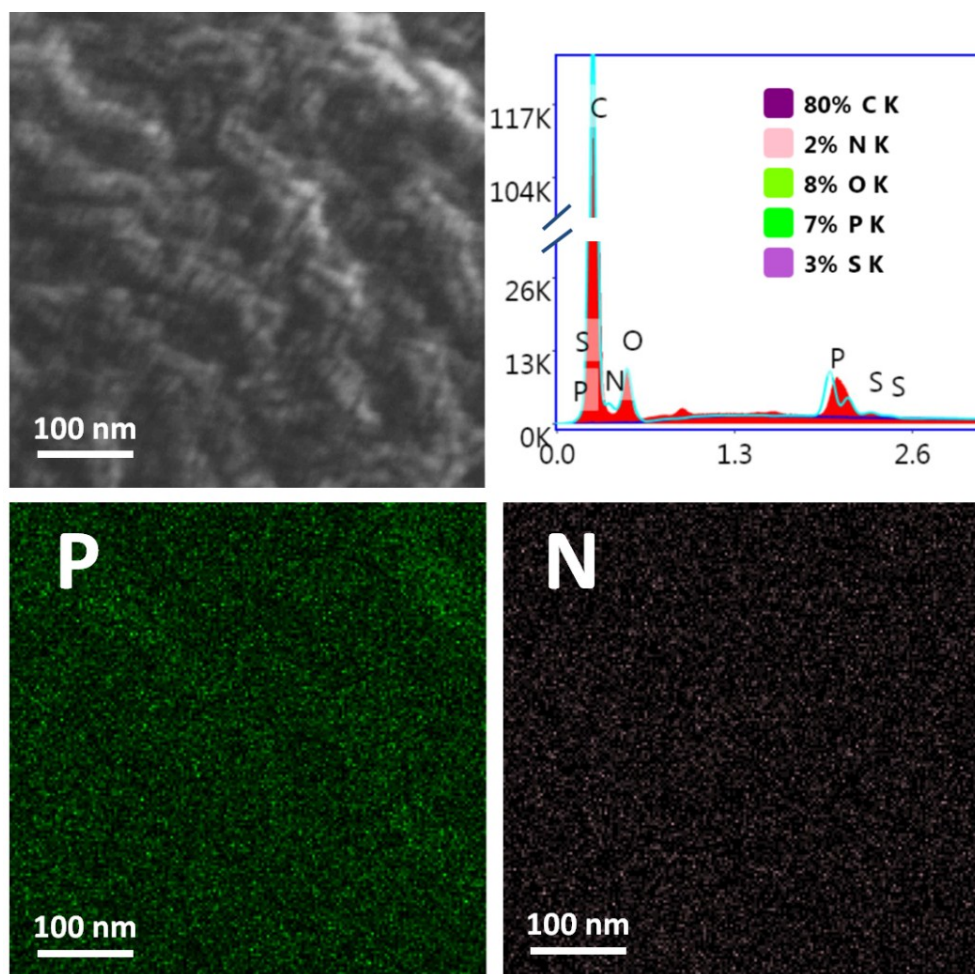


**Fig. S4.** EDS mapping of PIP-CSP<sub>6</sub>/TMC membrane.

It is clear from EDS mapping that nitrogen (N) and phosphorus (P) are evenly distributed on PIP-CSP<sub>6</sub>/TMC membrane, which confirms the presence of CSPs into the separation layer.

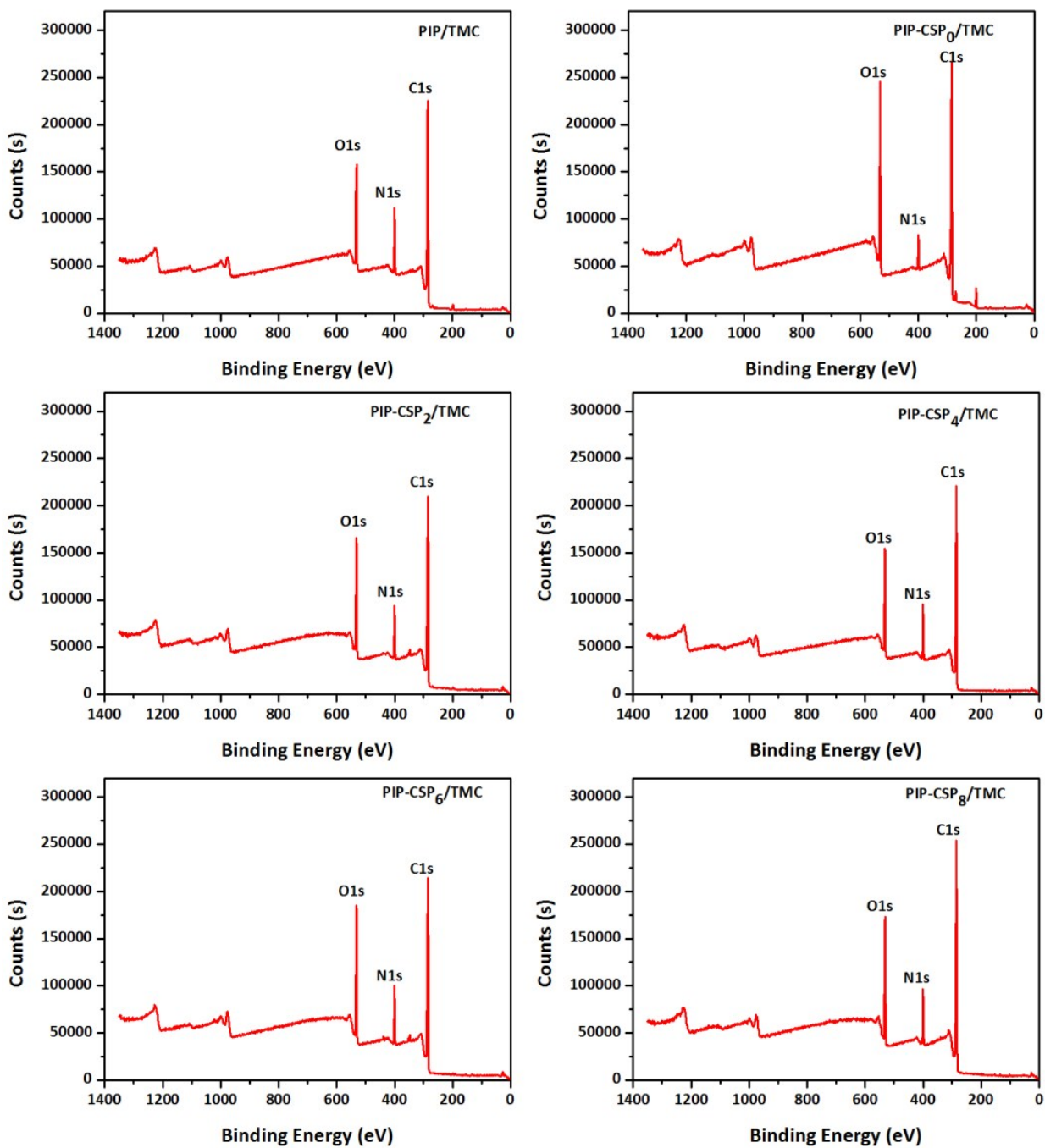
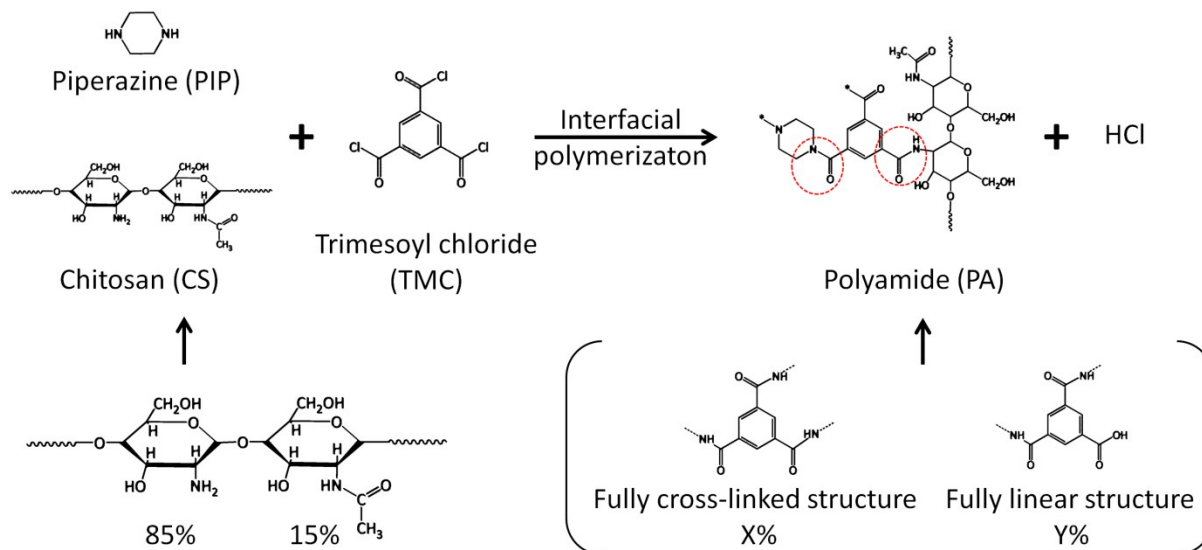


**Fig. S5.** XPS spectra of PIP/TMC and PIP-CSP/TMC membranes with different aging time.

## (8) Chemical Structure and Mechanism Diagram of Interfacial Polymerization



The molecular formula of CS with 85% of deacetylation degree is  $(\text{C}_{6.3}\text{H}_{11.3}\text{NO}_{4.15})_n$ .

**Fig. S6.** Mechanism diagram of interfacial polymerization, structural formulas of chitosan with 85% of deacetylation degree, and structural formulas of fully cross-linked polyamide and fully linear polyamide.

## (9) Calculating Crosslinking Degree of PA layer

**Note S1:** For PIP/TMC membrane, X% and Y% represent fully cross-linked polyamide and fully linear polyamide (Fig. S6), respectively. The degree of crosslinking (DC) based on amide bonds and carboxyls was derived from the following equation (1)<sup>1</sup>

$$\text{DC} = \frac{-\text{CONH}-}{(-\text{CONH}- + -\text{COOH}-)} \times 100\% \quad (1)$$

The ratio of nitrogen to oxygen was used to assist calculation and it obtained by the following equation (2)

$$\frac{-\text{CONH}-}{-\text{COOH}-} = \frac{2(\text{N/O})}{(1 - \text{N/O})} \quad (2)$$

Therefore, the degree of crosslinking was derived from the ratio of nitrogen-oxygen according to the following equation (3)

$$DC = 2(N/O)/(1 + (N/O)) \quad (3)$$

For example, without considering the participation of CS in the reaction, the N/O ratio of a fully cross-linked ( $X=100$ ) polyamide layer is 1.0 (repeated unit is  $C_{15}H_{15}N_3O_3$  without  $-COOH$  group) and the degree of crosslinking (DC) is 100%. The N/O ratio of a fully linear ( $Y=100$ ) polyamide layer is 0.5 (repeated unit is  $C_{13}H_{12}N_2O_4$  with one  $-COOH$  group) and the DC is 66.7%.

## (10) Hydrophilicity and Zeta Potential of the Membranes

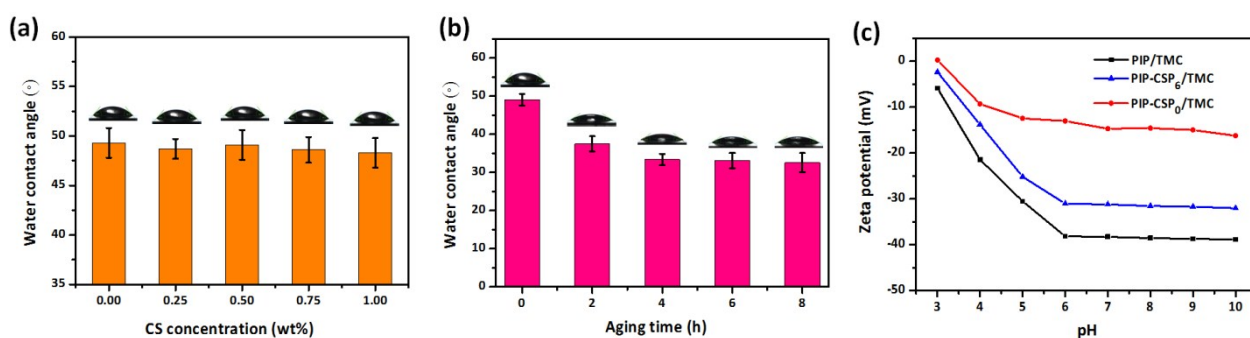


**Fig. S7.** Static water contact angles of PIP-CSP/TMC membranes with different concentration of chitosan on aging 0 h (a) and different aging time of chitosan nanoparticles on 0.5 wt% CS (b). (c) Surface zeta potential of PIP/TMC, PIP-CSP<sub>0</sub>/TMC and PIP-CSP<sub>6</sub>/TMC membranes (examined with 0.01 M KCl solution).

Static water contact angles of PIP/TMC membrane is about  $49.3^\circ$  (Fig. S7a), similar to the result (about  $45^\circ$ ) reported in the literature.<sup>2</sup> PIP-CSP/TMC membranes with different CS concentration at aging time of 0 h are ranged in  $48^\circ - 50^\circ$ , suggesting that CS concentration had no effect on the contact angles (Fig. S7a). With prolonging aging time from 0 to 4 h, the contact angles of PIP-CSP/TMC membranes decreases from  $49.1^\circ$  to  $33.4^\circ$  and then keeps unchanged (Fig. S7b), which is

relative to the change of surface morphologies of PIP-CSP/TMC membrane. Fig. S7c shows the change of the surface zeta-potential. PIP-CSP<sub>6</sub>/TMC and PIP/TMC membrane were all negatively charged in the pH range of 3-10 and the electronegativity was almost kept stable when pH value was larger than 6. This is because the remaining acyl chloride will be hydrolyzed into carboxylic acid after interfacial polymerization. With the increase of pH, the ionization of carboxylic acid is enhanced, showing stronger electronegativity. When the pH value is greater than 6, the ionization of carboxylic acid is basically completed, and the charge property of membrane tends to be stable,<sup>3-4</sup> so that the membrane potential remains constant in the pH range of 6-10. This phenomenon is consistent with the literatures.<sup>5-6</sup> PIP-CSP<sub>6</sub>/TMC membrane had less negative charges than PIP/TMC membrane because of the induction of CS molecules and CSPs with positive charges.

## (11) Cross-sectional Morphologies of Membranes

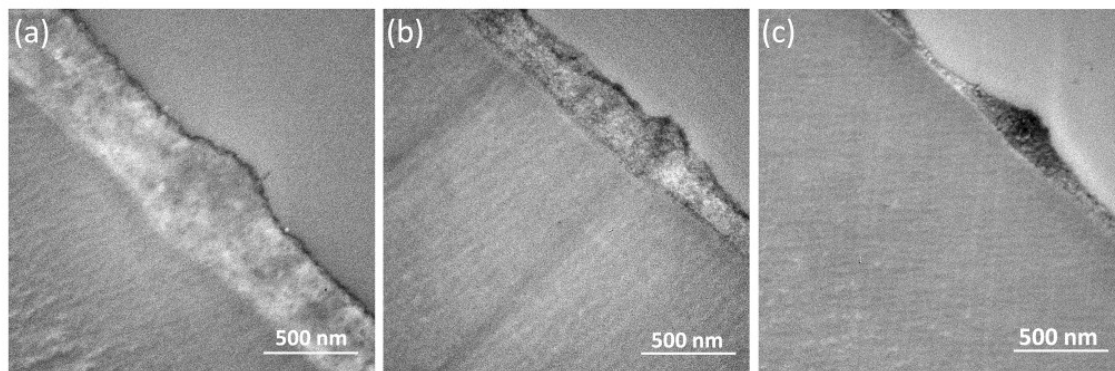


**Fig. S8.** Cross-sectional morphologies of membranes by TEM: (a) PIP-CSP<sub>2</sub>/TMC, (b) PIP-CSP<sub>4</sub>/TMC, and (c) PIP-CSP<sub>8</sub>/TMC membranes.

## (12) Relationship between Viscosity of Aqueous Amine Solution and the Thickness of PA Active Layer Obtained

**Note S2:** Freger et al. summarized the kinetic model of PA active layer formed by interfacial polymerization, and demonstrated that the thickness of PA active layer is governed by the local concentration of diamine monomers and the diffusion rate of diamine monomers entering organic phase.<sup>7</sup> From the Freger's kinetic model mentioned above, the PA layer thickness ( $\delta$ ) can be approximately calculated as follows:

$$\delta \sim [DL/k(f_a C_a + f_b C_b)]^{1/3} \quad (4)$$

where  $L$  (m) was the thickness of interface diffusion boundary layer;  $D$  ( $\text{m}^2 \cdot \text{s}^{-1}$ ) was the diffusivity of amine monomers entering the organic phase;  $k$  ( $\text{L} \cdot \text{mol}^{-1} \cdot \text{s}^{-1}$ ) was the reaction rate constant between the two monomers;  $C_a$  ( $\text{mol} \cdot \text{L}^{-1}$ ) and  $C_b$  ( $\text{mol} \cdot \text{L}^{-1}$ ) were the equilibrium concentration of amine monomers at the organic side and acryl chloride monomers in the organic phase, respectively;  $f_a$  and  $f_b$  were the functionality of amine monomer and acryl chloride monomer.<sup>8</sup>

The relationship between diffusion coefficient of particles and viscosity is described as follows:<sup>9</sup>

$$D = K_B T / 6\pi\eta_{macro} R \quad (5)$$

Where  $D$  is diffusion coefficient,  $K_B$  is Boltzmann constant,  $\eta_{macro}$  is viscosity and  $R$  is radius of particle.

From the equations (4) and (5), the thickness of PA layer is proportional to the third power of diffusion coefficient; and diffusion coefficient is inversely proportional to viscosity. So the high viscosity of solution leads to a thin PA layer in our work when the monomers' concentration is the same. This also explains why the thickness of the PA layer at different aging time is the same due to almost the same viscosity of the amine solution at different aging time mentioned in the

manuscript.

### (13) Experiment Setup of Membrane Separation and Pore Size of Membranes

**Note S3:** The separation performance evaluation of membranes was carried out by using a cross-flow system and the schematic diagram as shown in Fig. S9a. The effective area of the membrane was fixed at 7.1 cm<sup>2</sup>.

The pore size of membrane was determined by filtration of a group of polyethylene glycol (PEG) molecules with different molecular weights (200, 400, 600, 800 and 1000 Da, respectively). Rejection was calculated from the contents of total organic carbon (TOC) of feed and permeate solutions, respectively, as obtained by a TOC Analyzer. MWCO was obtained according to the molecular weight where the rejection is 90%. Stokes radius of PEG can be calculated according to its average molecular weight based on the following equation (6):

$$r_p = 16.73 \times 10^{-12} \times M^{0.557} \quad (6)$$

where  $M$  is molecular weight of solutes, and  $r_p$  is the Stokes radius.

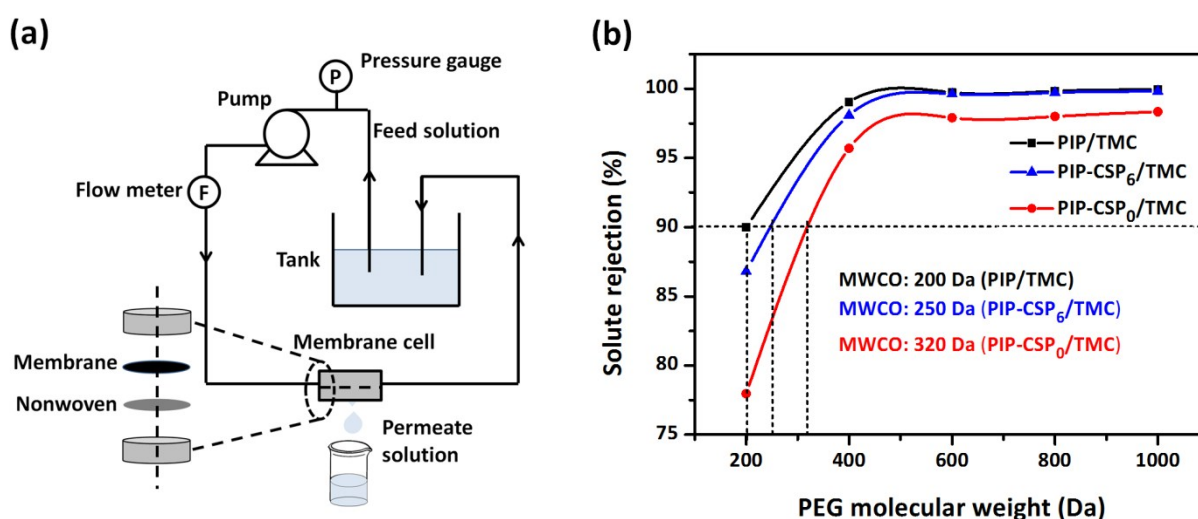


**Fig. S9.** (a) Schematic diagram of the cross-flow experimental setup. (b) Rejection curves to PEG with different molecular weight (1 g/ L PEG under 5 bar).

## (14) Separation Performance to Different Inorganic Salts

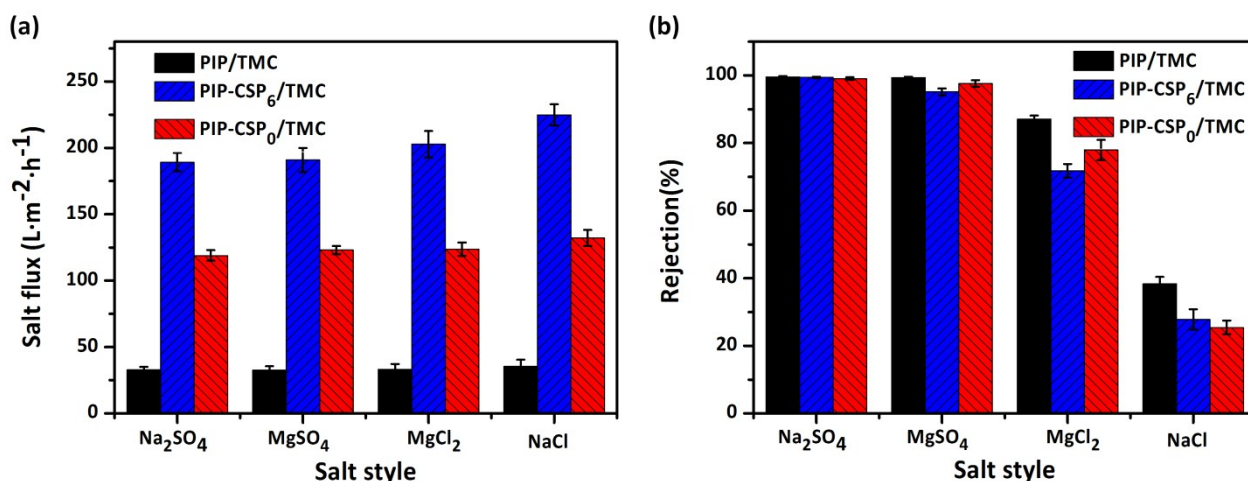


**Fig. S10.** Separation performance of PIP/TMC, PIP-CSP<sub>0</sub>/TMC, PIP-CSP<sub>6</sub>/TMC membranes to different inorganic salts (1 g/ L salt solution under 5 bar).

As shown in Fig. S10, the salt rejections of PIP/TMC, PIP-CSP<sub>0</sub>/TMC and PIP-CSP<sub>6</sub>/TMC membranes all follows the order: Na<sub>2</sub>SO<sub>4</sub> > MgSO<sub>4</sub> > MgCl<sub>2</sub> > NaCl, This is because membranes potential are mostly remained negatively charged in the pH range of 3–10. According to Donnan effect, the repulsion of SO<sub>4</sub><sup>2-</sup> is stronger than Cl<sup>-</sup>, and the rejection rate of MgSO<sub>4</sub> is higher than MgCl<sub>2</sub>. Combined with size exclusion effect, the hydrated radius of Mg<sup>2+</sup> (about 0.428 nm), is larger than Na<sup>+</sup> (about 0.358 nm), so that the rejection rate of MgCl<sub>2</sub> is higher than that of NaCl. In our work, the four salt rejection rates of the PIP-CSP/TMC membrane were all lower than PIP/TMC membrane, which was caused by the decrease of electronegativity and the increase of Stokes pore radius after the introduction of positively charged chitosan. Notably, the Stokes pore radius of PIP-

CSP<sub>0</sub>/TMC membrane (0.42 nm) is larger than PIP-CSP<sub>6</sub>/TMC membrane (0.36 nm), because more CS bunches existed in the PA layer in PIP-CSP<sub>0</sub>/TMC membrane, leading to a slight looser layer compared with PIP-CSP<sub>6</sub>/TMC membrane. But long CS chains in PIP-CSP<sub>0</sub>/TMC membrane attached on the membrane surface partly covered the membrane pores, leading to a lower permeance than that of PIP-CSP<sub>6</sub>/TMC membrane. The rejection rate of Mg<sup>2+</sup> salt in PIP-CSP<sub>0</sub>/TMC membrane is slightly higher than PIP-CSP<sub>6</sub>/TMC membrane. It is due to the more positive charged chitosan on the PIP-CSP<sub>0</sub>/TMC membrane surface reducing the attraction of Mg<sup>2+</sup> on the basis of Donnan effect.

## (15) Effect of pH of Feed Solution on Salt Separation Performance

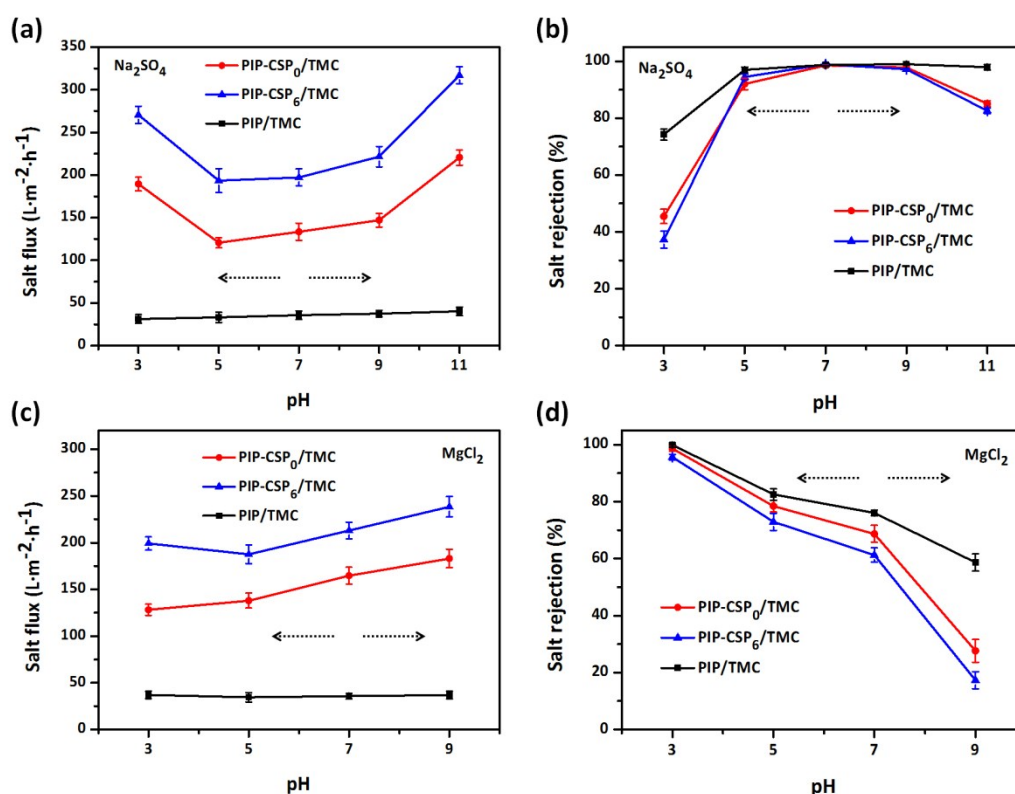


**Fig. S11.** Separation performance change of Na<sub>2</sub>SO<sub>4</sub> (a, b) and MgCl<sub>2</sub> (c, d) at different feed pH. Feed concentration: 1 g/L; operating pressure: 5 bar. The pH was adjusted by the addition of small amount of H<sub>2</sub>SO<sub>4</sub>, HCl and NaOH for Na<sub>2</sub>SO<sub>4</sub> and MgCl<sub>2</sub> feed solutions respectively.

As shown in Fig. S11, effect of pH on the performance of membrane was investigated.<sup>10-11</sup> For PIP-CSP<sub>6</sub>/TMC membranes, while the salt rejection of Na<sub>2</sub>SO<sub>4</sub> increases from 94.5% to 99.0% and to 97.2% with increasing feed pH from 5 to 7 and to 9. The salt flux is slightly increased. But the PIP-CSP/TMC membranes have a high salt flux and low rejection at pH=3 and pH=11, which may be caused by the destruction of the thin polyamide layer by strong acid or alkaline, or by the dissolution or leached out of chitosan.

And the salt rejection of MgCl<sub>2</sub> is still decreased from 98.7% to 27.7% with increasing feed pH from 3 to 9, with a slightly increased flux. This is because that the electronegativity enhances with

the increase of pH from the membrane potential (Fig. S7c), which helps to enhance the attraction to  $Mg^{2+}$  and the repulsion to  $SO_4^{2-}$ .<sup>12</sup>

From the above results, the PIP-CSP/TMC membranes could be more suitable to use in the pH range of 5-9.

## (16) Surface Roughness, Active Layer Thickness and Separation Performance of PIP/TMC, PIP-CSP<sub>0</sub>/TMC and PIP-CSP<sub>6</sub>/TMC Membranes

**Table S3**

The surface roughness, active layer thickness and separation performance of PIP/TMC, PIP-CSP<sub>0</sub>/TMC and PIP-CSP<sub>6</sub>/TMC membranes.

Membrane style	Surface roughness			Active layer thickness (nm)	Pure water permeate flux (L·m <sup>-2</sup> ·h <sup>-1</sup> )	Rejection of Na <sub>2</sub> SO <sub>4</sub> (%)
	Ra (nm)	Rq (nm)	Rz (nm)			
PIP/TMC	6.2	8.3	79.9	77±4	44.8	99.7
PIP-CSP <sub>0</sub> /TMC	4.4	5.6	42.3	23±6	140.7	99.1
PIP-CSP <sub>6</sub> /TMC	27.4	36.3	270	21±3	226.1	99.3

## (17) Mechanical Strength of Membranes

**Note S4:** The mechanical strength of membrane was evaluated by the change in performance after the membrane is pressurized to a pressure of 20 bar. The permeability and selectivity of the membrane were tested every 1 h at the same pressure and lasted for 3 h. It is found that increasing the pressure from 5 to 20 bar, the permeability maintained linear increase without sacrificing salt rejection. After that, when the pressure was reduced to 5 bar and then increased to 20 bar, the permeability and selectivity of the membrane restore to the corresponding values. All of the above results indicate that the membranes have good mechanical strength.<sup>10</sup>

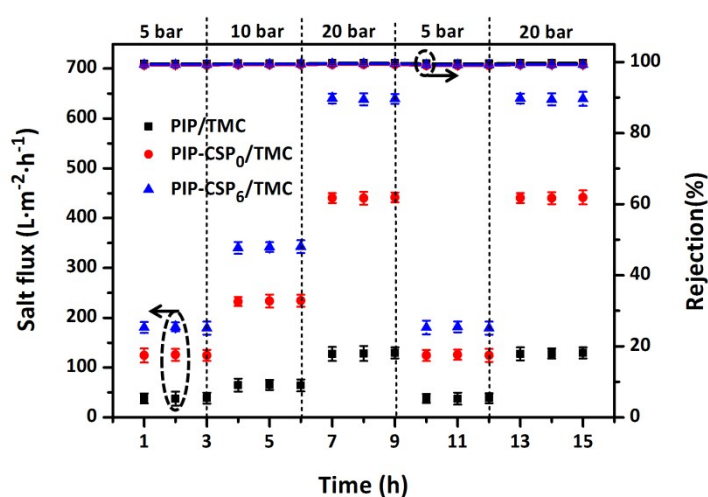


**Fig. S12.** Salt flux and rejection of Na<sub>2</sub>SO<sub>4</sub> by the membranes with time at each applied pressure under 1 g/L Na<sub>2</sub>SO<sub>4</sub> aqueous solution. The membranes kept running for 3 h at each pressure to obtain stable performance.

## (18) Comparison of Filtration Performance with NF membranes Reported in Literature and Commercial NF Membrane.

**Table S4**

Comparison of filtration performance with NF membranes in literature and commercial NF membrane.

Membranes	Pure water permeance ( $L \cdot m^{-2} \cdot h^{-1} \cdot bar^{-1}$ )	Na <sub>2</sub> SO <sub>4</sub> Rejection (%)	Reference
PIP-CSP <sub>6</sub> /TMC	45.2	99.3 (1000 ppm)	This work
PIP-PNPs/TMC	10.5	97.0 (1000 ppm)	13
PIP-ZNGs/TMC	10.6	97.8 (1000 ppm)	2
PIP-ZPNPs/TMC	11.0	96.0 (1000 ppm)	14
PIP-ZCNTs/TMC	14.9	97.0 (1000 ppm)	15
PIP-MWCNT-OH/TMC	6.9	97.6 (2000 ppm)	16
PIP-MWCNT-COOH/TMC	6.2	96.6 (2000 ppm)	16
PIP-MWCNT-NH/TMC	5.3	96.8 (2000 ppm)	16
PIP-ZIF-8/TMC	9.2	95.0 (1000 ppm)	17
PIP-SiO <sub>2</sub> /TMC	9.5	97.3 (2000 ppm)	18
PIP-PD/SWCNTs/TMC	32.0	95.9 (1000 ppm)	19
PIP-CNC/TMC	34.0	97.6 (1000 ppm)	20
PIP-PD/ZIF-8/TMC	53.5	95.0 (1000 ppm)	21
PIP-TSII/TMC	24.8	99.6 (2000 ppm)	22
NF-90	7.0	99.1 (1000 ppm)	23
NF-270	16.0	98.1 (1000 ppm)	23

## (19) Stability Evaluation

**Note S5. Stability evaluation:** The membrane samples were compacted for 30 minutes at 6 bar and then kept it stable for 10 minutes at 5 bar. Next, the permeated solution was collected with variation of time to test the stability of membrane.

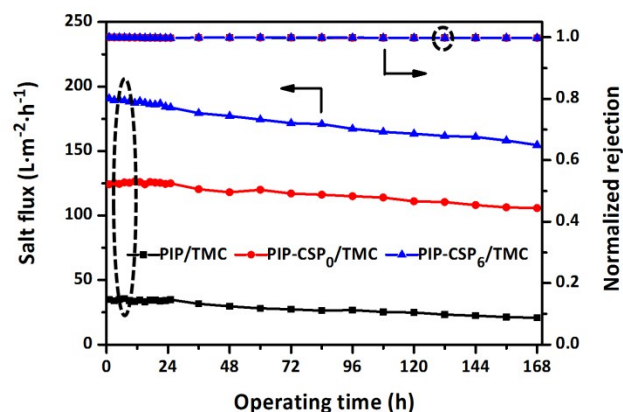


**Fig. S13.** Stability performance of PIP/TMC, PIP-CSP<sub>0</sub>/TMC and PIP-CSP<sub>6</sub>/TMC membranes tested with Na<sub>2</sub>SO<sub>4</sub> solution (1 g/L) for one week at 5 bar.

**Note S6. Membrane stability under different pH:** In order to evaluate the pH stability of membranes, soaked the membranes in the solution for 36 h under the acidic (pH = 3), neutral (pH = 7) and alkaline (pH = 11) conditions, respectively. And then, the pure water flux and Na<sub>2</sub>SO<sub>4</sub> rejection of the membrane were tested under 5bar.

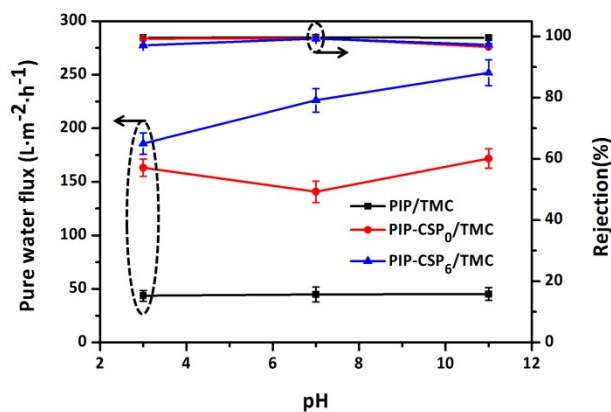


**Fig. S14.** The pure water flux and Na<sub>2</sub>SO<sub>4</sub> rejection of the membranes after soaking in the solution for 36 h under the acidic (pH = 3), neutral (pH = 7) and alkaline (pH = 11) conditions at 5 bar, respectively. The pH was adjusted by the addition of small amount of H<sub>2</sub>SO<sub>4</sub> and NaOH for deionized water respectively.

For PIP/TMC membrane, the pure water flux (about 44.8 L·m<sup>-2</sup>·h<sup>-1</sup>) and rejection of Na<sub>2</sub>SO<sub>4</sub> (about 99.7%) remained unchanged after soaking for 36h in the solution of pH=3, pH=7, and pH=11.

For PIP-CSP<sub>0</sub>/TMC membrane, the pure water flux increased from 140.7 L·m<sup>-2</sup>·h<sup>-1</sup> to 163.2 L·m<sup>-2</sup>·h<sup>-1</sup>, and the Na<sub>2</sub>SO<sub>4</sub> rejection (99.1%) remained unchanged after soaking for 36h in the solution from pH =7 to pH=3. It is believed that the dissolution of small amount of free chitosan molecules in the surface pores of membrane increased the permeability without destroy the selectivity under acidic condition. In addition, the pure water flux increased distinctly from 140.7 L·m<sup>-2</sup>·h<sup>-1</sup> to 171.8 L·m<sup>-2</sup>·h<sup>-1</sup>, and the Na<sub>2</sub>SO<sub>4</sub> rejection reduced from 99.1% to 96.6% after soaking for 36h in the solution from pH =7 to pH=11. This is because the gelation of free chitosan molecules in the surface pores of membrane under alkaline condition and increasing the pore diameter of membrane, increased the permeability and decreasing the selectivity of membrane.

For PIP-CSP<sub>6</sub>/TMC membrane, the pure water flux decreased from 226.1 L·m<sup>-2</sup>·h<sup>-1</sup> to 185.7 L·m<sup>-2</sup>·h<sup>-1</sup>, and the Na<sub>2</sub>SO<sub>4</sub> rejection was reduced from 99.3% to 97.1% after soaking for 36h in the solution of pH=3. It is attributed to the fact that free chitosan molecules in the surface pores of membrane can be swelling or even dissolve under acidic condition, which decreases the permeability and the selectivity of membrane. in addition, the pure water flux increased distinctly from 226.1 L·m<sup>-2</sup>·h<sup>-1</sup> to 251.8 L·m<sup>-2</sup>·h<sup>-1</sup>, and the Na<sub>2</sub>SO<sub>4</sub> rejection reduced from 99.3% to 97.3%

after soaking for 36h in the solution from pH=7 to pH=11. This is because the gelation of some free chitosan molecules in the surface pores of membrane under alkaline condition and increased the pore diameter of membrane, increasing the permeability and decreasing the selectivity of membrane.

From the above results, the PIP-CSP/TMC membranes should have a proper pH range.

## (20) Relationship between Aqueous Amine Solution with Different pH and Separation Performance of the Corresponding Membranes

**Table S5**

Aqueous amine solution with different pH and the separation performance of the corresponding membranes.

Membrane samples	Composition of aqueous amine solution(g)						pH	Pure water flux (L·m <sup>-2</sup> ·h <sup>-1</sup> )	Rejection to Na <sub>2</sub> SO <sub>4</sub> (%)
	PIP	CS	HAc (2%v/v)	SPP (10mg/ml)	TEA	H <sub>2</sub> O			
(1) HAc-CS-PIP-SPP	2	0.5	99.5	20	-	-	6.07±0.1	140.7±10 (0h)	99.1
(2) HAc-CS-PIP	2	0.5	99.5	-	-	20	6.03±0.1	57.1±5	99.3
(3) HAc-PIP-SPP	2	-	99.5	20	-	0.5	5.96±0.1	55.6±5	97.6
(4) PIP	2	-	-	-	-	120	11.2±0.1	30.2±5	98.3
(5) PIP-SPP	2	-	-	20	-	100	11.3±0.1	35.1±5	99.7
(6) PIP-TEA	2	-	-	-	0.5	119.5	11.4±0.1	44.7±5	99.7
(7) HAc-CS-PIP-TEA	2	0.5	99.5	-	0.5	19.5	6.43±0.1	106.1±10	99.5

Other conditions to prepare NF membrane: 0.5 % (w/w) TMC n-hexane solution react for 30 s at 25 °C.

## (21) Antifouling Property Evaluation

**Note S7.** *Antifouling properties evaluation:* Antifouling property of the membranes was measured as follows: first, deionized water through the membrane for 100 min, and then 1000 mg/L bovine serum albumin (BSA) was examined for the next 100 min. The BSA solution was prepared by

dissolving bovine serum protein in phosphate buffer solution containing  $\text{KH}_2\text{PO}_4$  (0.24 g/L) and  $\text{Na}_2\text{HPO}_4$  (1.44 g/L). After that, the feed solution was replaced by deionized water and the contaminants and salt on the membrane were removed through physical cleaning without applied pressure at a cross-flow velocity of 0.51 m/s for 1 h.<sup>24</sup> After the cleaning process begins, the cleaning solution was drained and fresh deionized water was replaced every 20 minutes to continue cleaning the membrane under the same conditions. The washing time was not counted in the filtration plots. A filtration cycle was defined as follows: 100 min filtration for deionized water and another 100 min filtration for bovine serum albumin. The anti-fouling performance of the membranes was assessed for 3.5 cycles. In order to evaluate the fouling resistance ability of membranes, flux recovery ratio (FRR) was calculated using the following equation (7):

$$FRR (\%) = J_c/J_0 \times 100\% \quad (7)$$

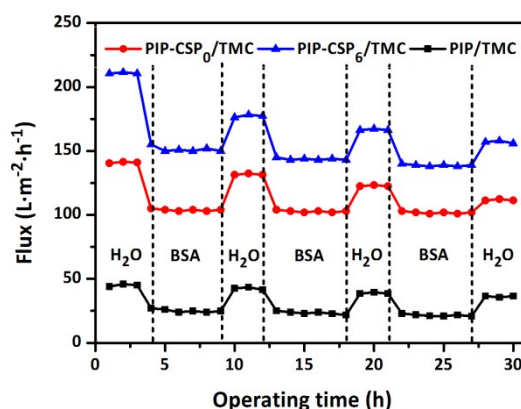


**Fig. S15.** Antifouling performance of PIP/TMC, PIP-CSP<sub>0</sub>/TMC and PIP-CSP<sub>6</sub>/TMC membranes tested with deionized water and 1000 mg/L bovine serum albumin (BSA) solution at 5 bar, respectively.

Antifouling performance was shown in Fig. S15, the flux of all the membranes went through a

sharp decline after the BSA solution was fed into the tank, suggesting a large amount of BSA protein depositing on the membrane surface. After being cleaned by deionized water, the flux recovery value of the PIP-CSP<sub>0</sub>/TMC membrane was 93.7 %, and the flux recovery value of the PIP /TMC membrane was 93.5 %, which is better than the PA membrane reported in other literatures (FRR=83.5%)<sup>25-26</sup> due to its smooth surface (Ra=6.2). The flux recovery value of the PIP-CSP<sub>6</sub>/TMC membrane was 84.4 %, which is slightly better than the reported PIP/TMC membrane. After 3.5 cycles, the pure water flux of the three membranes was 158.4 L·m<sup>-2</sup>·h<sup>-1</sup> (PIP-CSP<sub>6</sub>/TMC), 112.9 L·m<sup>-2</sup>·h<sup>-1</sup> (PIP-CSP<sub>0</sub>/TMC) and 35.5 L·m<sup>-2</sup>·h<sup>-1</sup> (PIP /TMC), respectively, and the rejection rate of Na<sub>2</sub>SO<sub>4</sub> was maintained at 99%, showing good antifouling performance.

## (22) Antibacterial Property Evaluation

**Note S8.** *Antibacterial property evaluation:* A plate counting method was used to characterize the antibacterial property of membranes. In brief, 15 g peptone, 5 g beef extract and 5 g sodium chloride were added to 1000 ml deionized water, and adjust the pH with 1 mol/L NaOH to 7.5 to prepare Lysogeny Broth (LB) liquid medium. The bacteria were inoculated in 250 mL LB liquid medium and cultivated in an incubator shaker at 37 °C and 120 rpm for 24 h. Next, 1 ml bacterial suspension was diluted with 100ml LB liquid medium and incubated for 18 h to enhance the activity of bacteria. The active suspension was 100-fold diluted with LB liquid medium and PBS (7.16 g/L Na<sub>2</sub>HPO<sub>4</sub>·12H<sub>2</sub>O, 1.36 g/L KH<sub>2</sub>PO<sub>4</sub>), successively. After that, the PES/SPSf, PIP/TMC and PIP-CSP/TMC membranes (0.75 g, 5 mm × 5 mm) sterilized by ultraviolet radiation were immersed into a flask with 5 mL diluted bacteria suspension and 70 mL PBS and then the mixture was cultured in an incubator shaker (150 rpm) at 37 °C for 18 h. After the incubation process, the sterile LB culture mediums were coated with 0.1 ml diluted bacteria suspension and incubated at 37 °C for 48 h. Finally, the colonies were counted from the agar plate, and antibacterial rate (Y) was defined by the following equation (8):

$$Y(\%) = (N_b - N_s)/N_b \times 100\% \quad (8)$$

Where  $N_b$  and  $N_s$  are representing the numbers of viable bacteria colonies were counted from the agar plate treated with the PIP/TMC membrane and the PIP-CSP/TMC membranes, respectively.

As shown in Fig. S16, the PIP-CSP/TMC membrane showed better antibacterial property of *E. Coli*, higher 78.8 % than PIP/TMC membrane due to CS existence.<sup>27</sup>

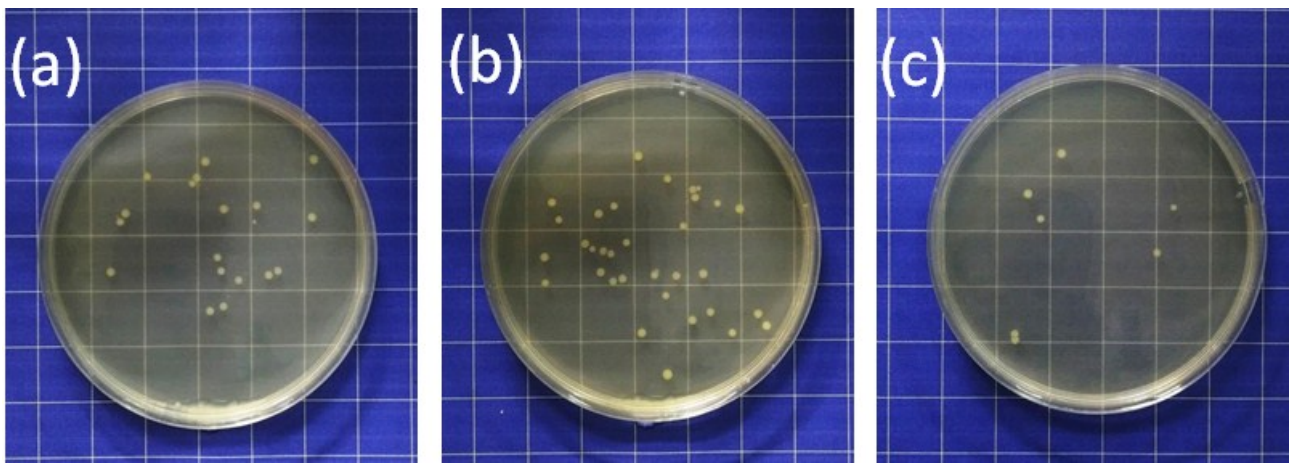


**Fig. S16.** Photographs of *E. coli* colonies on the agar plate related to (a) PES/SPSf, (b) PIP/TMC and (c) PIP-CSP/TMC membranes.

## References

- 1 Y. Liu, B. Q. He, J. X. Li, R. D. Sanderson, L. Li, S. B. Zhang, *J. Membr. Sci.*, 2011, **373**, 98-106.
- 2 Y. L. Ji, Q. F. An, X. D. Weng, W. S. Hung, K. R. Lee, C. J. Gao, *J. Membr. Sci.*, 2018, **548**, 559-571.
- 3 S. Gorgieva, V. Kokol, *Carbohydr. Polym.*, 2011, **85**, 664-673.
- 4 M. F. Abou Taleb, H. L. A. El-Mohdy, H. A. A. El-Rehim, *J. Hazard. Mater.*, 2009, **168**, 68-75.
- 5 P. Wen, Y. B. Chen, X. Y. Hu, B. W. Cheng, D. Q. Liu, Y. F. Zhang, S. Nair, *J. Membr. Sci.*, 2017, **535**, 208-220.
- 6 M. B. Wu, Y. Lv, H. C. Yang, L. F. Liu, X. Zhang, Z. K. Xu, *J. Membr. Sci.*, 2016, **515**, 238-244.
- 7 V. Freger, S. Srebnik, *J. Appl. Polym. Sci.*, 2003, **88**, 1162-1169.
- 8 M. Wu, J. Yuan, H. Wu, Y. Su, H. Yang, X. You, R. Zhang, X. He, N. A. Khan, R. Kasher, Z. Jiang, *J. Membr. Sci.*, 2019, **576**, 131-141.
- 9 Y. Cheng, R. K. Prud'homme, J. L. Thomas, *Macromolecules*, 2002, **35**, 8111-8121.
- 10 J. S. Trivedi, D. V. Bhalani, G. R. Bhadu, S. K. Jewrajka, *J. Mater. Chem. A*, 2018, **6**, 20242-20253.
- 11 A. Bera, J. S. Trivedi, S. K. Jewrajka, P. K. Ghosh, *J. Membr. Sci.*, 2016, **519**, 64-76.
- 12 S. Y. Kim, S. M. Cho, Y. M. Lee, S. J. Kim, *J. Appl. Polym. Sci.*, 2000, **78**, 1381-1391.
- 13 Y. Ji, W. Qian, Q. An, K. r. Lee, C. Gao, *J. Ind. Eng. Chem.*, 2018, **66**, 209-220.
- 14 Y. L. Ji, Q. F. An, Y. S. Guo, W. S. Hung, K. R. Lee, C. J. Gao, *J. Mater. Chem. A*, 2016, **4**,

4224-4231.

- 15 J. F. Zheng, M. Li, Y. J. Yao, X. Zhang, L. J. Wang, *J. Mater. Chem. A*, 2017, **5**, 13730-13739.
- 16 S. M. Xue, Z. L. Xu, Y. J. Tang, C. H. Ji, *ACS Appl. Mater. Interfaces*, 2016, **8**, 19135-19144.
- 17 F. Xiao, B. Wang, X. Hu, S. Nair, Y. Chen, *J. Taiwan Inst. Chem. Eng.*, 2018, **83**, 159-167.
- 18 D. Hu, Z.-L. Xu, C. Chen, *Desalination*, 2012, **301**, 75-81.
- 19 Y. Z. Zhu, W. Xie, S. J. Gao, F. Zhang, W. B. Zhang, Z. Y. Liu, J. Jin, *Small*, 2016, **12**, 5034-5041.
- 20 J. J. Wang, H. C. Yang, M. B. Wu, X. Zhang, Z. K. Xu, *J. Mater. Chem. A*, 2017, **5**, 16289-16295.
- 21 Z. Y. Wang, Z. X. Wang, S. H. Lin, H. L. Jin, S. J. Gao, Y. Z. Zhu, J. Jin, *Nat. Commun.*, 2018, **9**, 2004-2013.
- 22 Z. Tan, S. Chen, X. Peng, L. Zhang, C. Gao, *Science*, 2018, **360**, 518-521.
- 23 X. Ma, H. Guo, Z. Yang, Z. Yao, W. Qing, Y. Chen, Z. Xu, C. Y. Tang, *J. Membr. Sci.*, 2019, **570**, 139-145.
- 24 Y. Mo, A. Tiraferri, N. Y. Yip, A. Adout, X. Huang, M. Elimelech, *Environ. Sci. Technol.*, 2012, **46**, 13253-13261.
- 25 M. Y. Wu, T. Y. Ma, Y. L. Su, H. Wu, X. D. You, Z. Y. Jiang, R. Kasher, *J. Membr. Sci.*, 2017, **544**, 79-87.
- 26 X. You, T. Ma, Y. Su, H. Wu, M. Wu, H. Cai, G. Sun, Z. Jiang, *J. Membr. Sci.*, 2017, **540**, 454-463.
- 27 Z. Wang, F. Yan, H. C. Pei, J. X. Li, Z. Y. Cui, B. Q. He, *Carbohydr. Polym.*, 2018, **198**, 241-248.